Received: 31 August 2022 | Revised: 28 September 2022 | Accepted: 4 October 2022

DOI: 10.1111/jace.18850

Journal of the American Ceramic Society

RESEARCH ARTICLE

Predicting initial dissolution rates using structural features from molecular dynamics simulations

Xiaonan Lu[1] | **Lu Deng**[2] | **Stéphane Gin**[3] | **Benjamin Parruzot**[1] | **Joelle T. Reiser**[1] | **Joseph V. Ryan**[1] | **John D. Vienna**[1] | **Jincheng Du**[2]

[1]Energy and Environment Directorate, Pacific Northwest National Laboratory, Richland, Washington, USA

[2]Department of Materials Science and Engineering, University of North Texas, Denton, Texas, USA

[3]CEA, DES, ISEC, DE2D, Université de Montpellier, Bagnols-sur-Cèze Cedex, France

Correspondence
John D. Vienna, Energy and Environment Directorate, Pacific Northwest National Laboratory, Richland, WA 99352, USA.
Email: John.Vienna@pnnl.gov

Jincheng Du, Department of Materials Science and Engineering, University of North Texas, Denton, TX 76203, USA.
Email: Jincheng.Du@unt.edu

Funding information
U.S. Department of Energy (DOE), Office of Science, Basic Energy Sciences, Grant/Award Number: # DESC0016584

Abstract

Predicting the chemical durability of glass materials is important for various applications from daily life such as cell phone screens and kitchenware to advanced technologies such as nuclear waste disposal and biomedicine. In this work, we explored the prediction of the initial glass dissolution rates using structural features from molecular dynamics (MD) simulations for a series of glass compositions (total 28), including ZrO_2- and V_2O_5-containing boroaluminosilicate, borosilicate, and aluminosilicate glasses. The initial dissolution rates (r_0) measured experimentally at 90°C with varying solution conditions were correlated with structural features (e.g., polyhedral linkages and non-bridging oxygen species) obtained from MD simulations, either from this study or from literature. As hydrolysis of the glass network through breaking of the network former linkages (e.g., Si–O–Si, Si–O–Al, etc.) is a critical step of network glass dissolution, the statistics of these linkages obtained from MD were also correlated to r_0 through linear regression, where the coefficients of determination (R^2) and root mean square error are found to be 0.949 and 0.681, respectively. This model was compared and discussed with existing models developed by various approaches, including machine learning, the kinetic rate equation, topological constraint theory, and other descriptors from MD simulations. The discussion provides insights on future model improvements to predict glass dissolution. In addition, as the effect of V_2O_5 on glass dissolution was not well studied comparing to ZrO_2, the impact of V_2O_5 was emphasized in this paper, suggesting that the impact is not the same across all glass compositions and test conditions.

KEYWORDS
atomistic simulation, glass dissolution, polyhedral linkage, vanadium oxide

1 | INTRODUCTION

Glass materials are important for day-to-day life (e.g., cell phone screens, kitchenware, and buildings), in the biomedical fields (e.g., bioactive glass coatings on metallic implants), and for national missions (e.g., nuclear waste disposal and electrodes/interconnects for energy storage). Being able to have controllable glass durability is important for various industrial and technological applications. For example, bioactive glasses desire a relatively fast and stable dissolution, whereas nuclear waste glasses need long-term stability and durability.[1–3] Generally, the kinetics of glass corrosion can be divided into three stages (initial rate, residual rate, and accelerated rate).[4–6] However, predicting the dissolution behavior of glasses is complicated, as glass corrosion not only depends on the bulk glass composition and structure, but is also affected by various external parameters, such as pH,[7–9] temperature,[10,11] and solution composition.[12–17] In this paper, we focus on quantifying the relationship between glass structure and initial dissolution rate (r_0, also commonly known as forward rate), where the rate is mostly dependent on glass composition, temperature, and pH, as compared to the residual or resumption rate which are strongly affected by near field materials and solution feedback. Note that an effort has been made to distinguish initial dissolution rate and forward rate by Thorpe et al.,[18] where forward rate has no solution feedback as it is measured in flow-through conditions or very dilute conditions, initial dissolution rates are measured at early reaction progress before solution feedback is measurable with changing solution pH being acceptable. By this definition, the rates discussed in this paper are initial dissolution rates.

An effective method to measure r_0 is to dissolve glasses in sufficiently dilute conditions so there is no impact from solution feedback, whereas the solution being concentrated enough with glass components so reliable quantitative analyses can be obtained.[10] Various methods were developed to measure r_0, including static tests,[19] single-pass flow-through (SPFT, ASTM Method C1662[20]), and microchannel flow-through (MCFT[7]) tests. The International Simple Glass (ISG) has served as a model or reference glass for studies on the corrosion mechanisms of nuclear waste glass through active international collaborations since it was introduced in 2013.[4,21] Despite using samples of the standard glass from the same batch, the measured dissolution rates of ISG show variations depending on the testing method, solution pH, temperature, and sample forms. Inagaki et al.[7] measured the r_0 of ISG as a function of pH (3–10) and temperature (20–90°C) using MCFT, and the r_0 of $pH_{90°C}$ = 3 and $pH_{90°C}$ = 10 are 0.978 ± 0.061 and 7.65 ± 0.17 g m^{-2} d^{-1}, respectively. The r_0 of ISG was found to be 8.2 ± 2.5 g m^{-2} d^{-1} measured under static conditions at $pH_{90°C}$ = 9 by Gin et al.,[22] whereas a dissolution rate of 5.44 g m^{-2} d^{-1} at 90°C with $pH_{22°C}$ = 11 was obtained using SPFT by Neeway et al.[23] Fournier et al.[19] systematically evaluated the r_0 measurements on ISG using static, SPFT, and MCFT at 90°C and $pH_{90°C}$ = 10. It was observed that r_0 of ISG is between 5 and 17 g m^{-2} d^{-1}, depending on the measurement methods, sample form (powders or monoliths), and glass surface area analysis method (Brunauer–Emmett–Teller method or geometric surface). Even though the r_0 measurements (at 90°C and $pH_{90°C}$ = 10) have a clear repeatability, the results should be given with an uncertainty of ~±25%.[19]

Many studies have been conducted to correlate glass dissolution from intrinsic and extrinsic parameters using regression models,[10] topological constraint theory (TCT),[22,24,25] machine learning,[26–29] and molecular dynamics (MD) simulation-based quantitative structure–property relationship (QSPR) analysis.[30–33] Vienna et al.[10] showed that 90% of the variation in r_0 data can be explained by variations in pH and temperature, where compositional effects are relatively small within the range of glasses used in waste vitrification. A structural descriptor based on the TCT was developed by Gin et al.,[22] which can be used to predict the r_0 of aluminosilicate and borosilicate glasses that dissolve congruently at 90°C and $pH_{90°C}$ = 9. MD-based QSPR analysis is also a powerful approach to correlate macroscopic properties with microstructure and chemical features.[34] A structural descriptor (F_{net}) that combines short-range structural and energetic information has been developed and used to correlate glass parameters, such as r_0,[32,33] thermal properties, and mechanical properties.[35] In a study by Du and Rimsza,[36] the energy barrier for breakage of network former linkages (i.e., former–oxygen–former) under different reaction conditions from literature were summarized and compared, showing the energy barriers for hydrolysis of these linkages is mainly a function of the protonated, neutral, and deprotonated conditions, consistent with experiments, but the results also show fairly large variations depending on the theoretical levels (of quantum mechanical calculation) and type of models (cluster versus periodic) used. As hydrolysis is a critical step of glass dissolution and the stability of the glass former linkages is affected by pH and other parameters, we aim to use the statistics of these linkages obtained from MD simulations to correlate with the initial dissolution rate measured experimentally.

The main objective of this work is to develop models using key structural features obtained from MD simulations to predict r_0 measured at 90°C with different pH, providing insights on future model development. In addition, a series of V_2O_5-containing boroaluminosilicate glasses

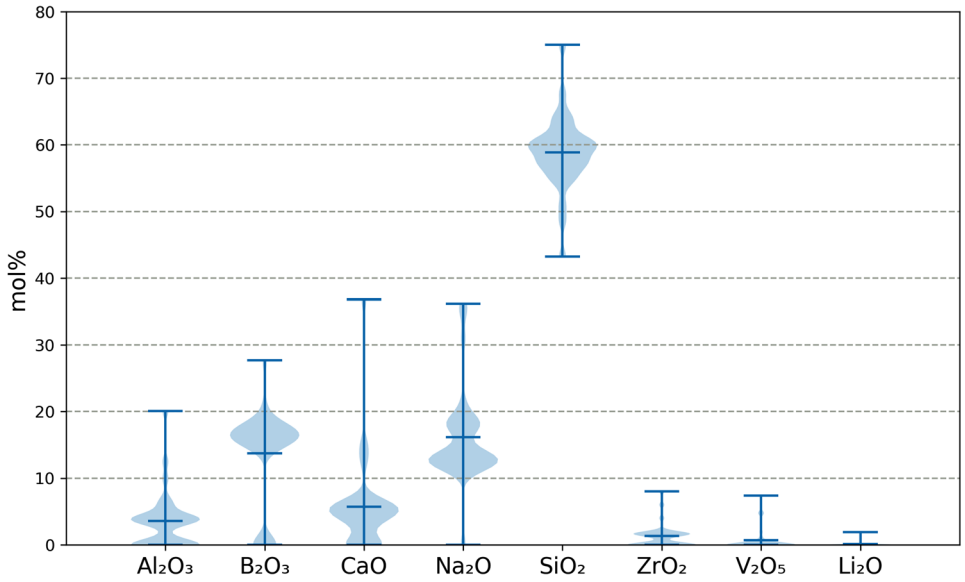

FIGURE 1 Violin plot showing the distribution of glass compositions with maximum, average, and minimum value labeled

were included and studied in this work, as these glass materials have attracted great interest due to their potential applications, such as lithium ion batteries,[37,38] and as nuclear waste forms with increased sulfur solubility.[39–43] The impacts of V_2O_5 on the properties of ISG have been investigated previously,[44] where the addition of V_2O_5 was found to decrease glass transition temperature (T_g) and hardness while increasing the refractive index and crack initiation load. It was previously found that vanadium mainly exists in two oxidation states in ISG-based glasses, ~80% V^{5+} (in four-, five-, and six-fold coordination) and ~20% V^{4+} (mainly in fourfold coordination), by an integrated experimental and MD simulation study.[45]

This paper is arranged as follows: methodology, including data collection, r_0 measurement, and model fitting; then the results on structural features obtained from MD, dissolution data, and a model to predict r_0 from the structural features (e.g., former linkages); and finally discussions relating the model to others in the literature and conclusions.

2 | METHODOLOGY

The 28 glasses studied (referred hereafter as the V series,[44,45] Zr series,[33,46] and CJ series[22,32]) were previously fabricated, characterized experimentally, and simulated using MD. Table 1 lists the glass compositions and the initial dissolution rates (r_0) both determined experimentally in this work and from references. Figure 1 shows the distribution of the 28 glass compositions with the maximum, average, and minimum values labeled. The r_0 values of V series were measured in this study following the procedure reported in Gin et al.[22] The test uses glass particles with diameters of 63–125 μm measured in aqueous solutions to achieve a surface area (geometric surface) to a solution volume ratio of 0.03 cm^{-1} (0.05 g glass and 500 ml solution) for $pH_{90°C} = 10$ and 0.14 cm^{-1} (0.05 g glass and 100 ml solution) for $pH_{90°C} = 2$.[22] These static testing conditions ensured that glass dissolution is controlled by the hydrolysis of the covalent bonds (i.e., Si–O–M with M = Si, Al, B, or Zr).[22] Hence, the release of Si represents glass matrix/network dissolution and is used to calculate the glass initial dissolution rate. The rest of the r_0 data (static tests) were taken from the previous experimental studies.

Details of MD simulations were reported previously,[32,33,45] and a brief description is presented here. Cubic simulation cells with ~12000 atoms (for the Zr and CJ series) and ~20000 atoms (for the V glass series) were generated with random initial configurations. The glass structures were then obtained through a simulated melt-and-quench process (from 6000 to 300 K) with a nominal cooling rate of 1 K ps^{-1} (CJ series), 2.5 K ps^{-1} (V series), or 1.4 K ps^{-1} (Zr series) using MD simulations. A set of partial charge pairwise potentials with long-range Coulombic interactions and short-range interactions with the Buckingham form[47] was used to simulate the multicomponent borosilicate glass systems with recently developed boron oxide parameters by Deng and Du.[48] Details of the potential form, composition-dependent boron potential, and parameters can be found in Ref. [48]. Vanadium-related parameters that are compatible with the above potentials can be found in Ref. [49]. The potentials have been successfully used to simulate a range of borosilicate and boroaluminosilicate glasses such as ISG and related systems.[32,33,45]

TABLE 1 Target glass composition (mol%), initial dissolution rates experimentally measured at different pH values, and studies that characterized (Exp. ref.) and simulated (molecular dynamics [MD] ref.) these glasses

MD ref.	Exp. refs.	Glass ID 1	Glass ID 2	Al_2O_3	B_2O_3	CaO	Na_2O	SiO_2	ZrO_2	V_2O_5	Li_2O	pH (90°C)	Si r_0, g m^{-2} d^{-1}
Lu et al.[45]	Lu et al.[44] and this study	ISG	ISG	3.84	15.96	5.73	12.65	60.20	1.62	–	–	10	17
		0.5V	0.5V	3.82	15.89	5.70	12.58	59.90	1.61	0.50	–	10	20
		1V	1V	3.81	15.81	5.67	12.52	59.60	1.60	0.99	–	10	22
		2V	2V	3.77	15.65	5.62	12.40	59.02	1.58	1.96	–	10	32
		5V	5V	3.66	15.20	5.46	12.04	57.34	1.54	4.76	–	10	71
		8V	8V	3.56	14.78	5.30	11.71	55.74	1.50	7.40	–	10	68
		ISG	ISG	3.84	15.96	5.73	12.65	60.20	1.62	–	–	2	0.86
		5V	5V	3.66	15.20	5.46	12.04	57.34	1.54	4.76	–	2	6.4
Lu et al.[33]	Cailleteau et al.[46]	0Zr	0Zr	–	17.00	4.00	18.00	61.00	–	–	–	6.9	37
		1Zr	1Zr	–	17.00	4.00	18.00	60.00	1.00	–	–	6.9	15
		2Zr	2Zr	–	18.00	4.00	18.00	59.00	2.00	–	–	6.9	5.1
		4Zr	4Zr	–	18.00	4.00	18.00	57.00	4.00	–	–	6.9	1.3
		6Zr	6Zr	–	17.00	4.00	18.00	55.00	6.00	–	–	6.9	0.19
		8Zr	8Zr	–	18.00	4.00	19.00	51.00	8.00	–	–	6.9	0.091
Du et al.[32]	Gin et al.[22]	CJ1	NBS14/18	–	18.00	–	14.20	67.70	–	–	–	9	14
		CJ2	NBSA	4.10	17.30	–	13.60	64.90	–	–	–	9	2.6
		CJ3	NBSAC	3.90	16.30	5.80	12.80	61.20	–	–	–	9	9.9
		CJ4 (ISG)	NBSACZ	3.80	16.00	5.70	12.60	60.10	1.70	–	–	9	8.2
		CJ7	NBSAZ	4.00	17.00	–	13.40	63.80	1.80	–	–	9	2.2
		CJ8	NBSC	–	17.00	6.00	13.40	63.60	–	–	–	9	52.2
		CJ9	NBSCZ	–	16.70	5.90	13.10	62.50	1.80	–	–	9	56.4
		NBS17-24	NBS12/28	–	27.70	–	11.60	60.50	–	–	–	9	197
		NBS35-19	NBS36/21	–	20.70	–	36.20	43.20	–	–	–	9	47,370
		NBS29-13	NBS31/15	–	15.00	–	30.90	54.20	–	–	–	9	2070
		–	NSAC19	9.90	–	13.90	19.00	55.30	–	–	1.90	9	6.1
		–	NSAC17	20.10	–	12.30	17.00	48.60	–	–	1.90	9	7.4
		–	NSAC21	5.90	–	15.40	21.30	57.40	–	–	–	9	6
		–	NSAC0	5.90	–	36.80	–	57.30	–	–	–	9	3.8
		–	NSAC35	6.90	–	–	34.90	58.10	–	–	–	9	1.2
		Albite glass	NSA	12.50	–	–	12.50	75.00	–	–	–	9	0.26

Note: A dash (–) indicated the element is absent from the glass.
Abbreviation: ISG, International Simple Glass.

TABLE 2 Estimated model coefficients, standard deviation of the coefficients, and model-fit summary statistics

Term	Coefficient estimate	Coefficient Stand. err.	Model statistic	Value
Intercept	2.38	1.85	Data points	28
pH (90°C)	0.91	0.19	R^2	0.949
Al–O–B	−30.09	9.00	RMSE	0.681
Al–O–Si	−11.14	0.98	R^2 adjusted	0.935
Si–O–Si	−16.74	1.74	R^2 press	0.887
Former–O–Zr	−29.49	2.84	RMSE press	0.877
NBO, %	0.14	0.02		

Abbreviations: NBO, non-bridging oxygen; RMSE, root mean square error.

Model fitting was performed using JMP version 14.0.0 (SAS Institute, Cary, NC). The model form (linear mixture) is described in the following equation:

$$\ln[r_0] = a_0 + \sum_{i=1}^{q} a_i x_i \quad (1)$$

where r_0 is the initial dissolution rate (g m^{-2} d^{-1}), a_0 is the intercept, a_i is the ith model term (e.g., fraction of former linkages, pH) coefficient, as listed in Table 2, x_i is the ith model term, and q is the number of the model components.

Models were fitted using r_0 measured between $pH_{90°C}$ of 6.9 and 10 (the data from $pH_{90°C} = 2$ were not used during model fitting, as discussed in Section 3.2). Guided by stepwise regression and knowledge of structural effect, the model parameters with the highest impacts were selected. Nonlinear (higher order) and mixing effects were also evaluated, but they were ultimately found to be insignificant.

3 | RESULTS

3.1 | MD structural features

Figure 2 shows a stacked bar chart of the polyhedral linkages of the studied glasses. The number of each polyhedral linkage can be found in the Supplementary Information (SI) section. For Zr series, r_0 ($pH_{90°C} = 6.9$) increases with decreasing former–O–Zr and increasing B–O–Si, whereas for V series, r_0 ($pH_{90°C} = 10$) increases with increasing former–O–V (except 8 V). There is no obvious trend between r_0 and the linkages for the CJ series as shown in Figure 2 ($pH_{90°C} = 9$).

3.2 | Dissolution results

Initial dissolution rate values (r_0) for the Zr and CJ series were previously published and discussed,[22,46] whereas the r_0 values of the V series were newly measured in this study. Figure 3 shows the normalized mass loss (NL) of Si for the V series tested at $pH_{90°C} = 10$ and 2, and the calculation of NL_{Si} with shrinking core model applied can be found in a previous study.[22] Equivalent thickness (calculated from NL divided by glass density) at $pH_{90°C} = 10$ can be found in the SI section, where the results indicate that all the glasses dissolved nearly congruently (Figure S1) and at the same rate (r_0) throughout all time points (as indicated by the linear behavior of the curves, see Figure 3A). At $pH_{90°C} = 10$, the NL_{Si} increases with increasing V_2O_5 concentration in glass, except that 5 and 8 V show the same NL_{Si}, and r_0 increased from 17 to 71 g m^{-2} d^{-1} (based on Si, as shown in Table 1). Although at $pH_{90°C} = 2$, nonlinear behavior is shown for the vanadium containing glass (Figure 3B). The 5 h NL_{Si} values for ISG and 5 V samples measured at $pH_{90°C} = 2$ are about 20 and 9 times smaller, respectively, than the values obtained at $pH_{90°C} = 10$. The r_0 values of ISG (based on Si) measured in this study are 17 ($pH_{90°C} = 10$) and 0.962 ($pH_{90°C} = 2$) g m^{-2} d^{-1} (Table 1), which are comparable with the previous findings[7,19] listed in Section 1.

Under acidic conditions, the incongruent dissolution of the glasses was observed as expected. The much smaller rate under acid condition (shown in Table 1 and Figure S3) was due to the fast formation of alteration layers, as well as modification of the hydrolysis energy for Si under acidic condition. Kaya et al.[50] observed a blueshift of the Si–O band after the loss of modifier ions as well as boron species from the glass network, which indicates that the depleted glass became closer to a more durable silica glass, leading to a resistance of the remaining glass network to further hydrolysis. Figure 4 shows the equivalent thickness of Si, B, Na, Al, Ca, and V tested at $pH_{90°C} = 2$. The dissolution behavior of ISG and to a lesser extent that of 5 V indicate that there is a rate change over time, particularly between the first and second hours. These observations suggest that ISG and 5 V did not dissolve at r_0 throughout the entire experiment; therefore, these data were excluded from model fitting in this paper.

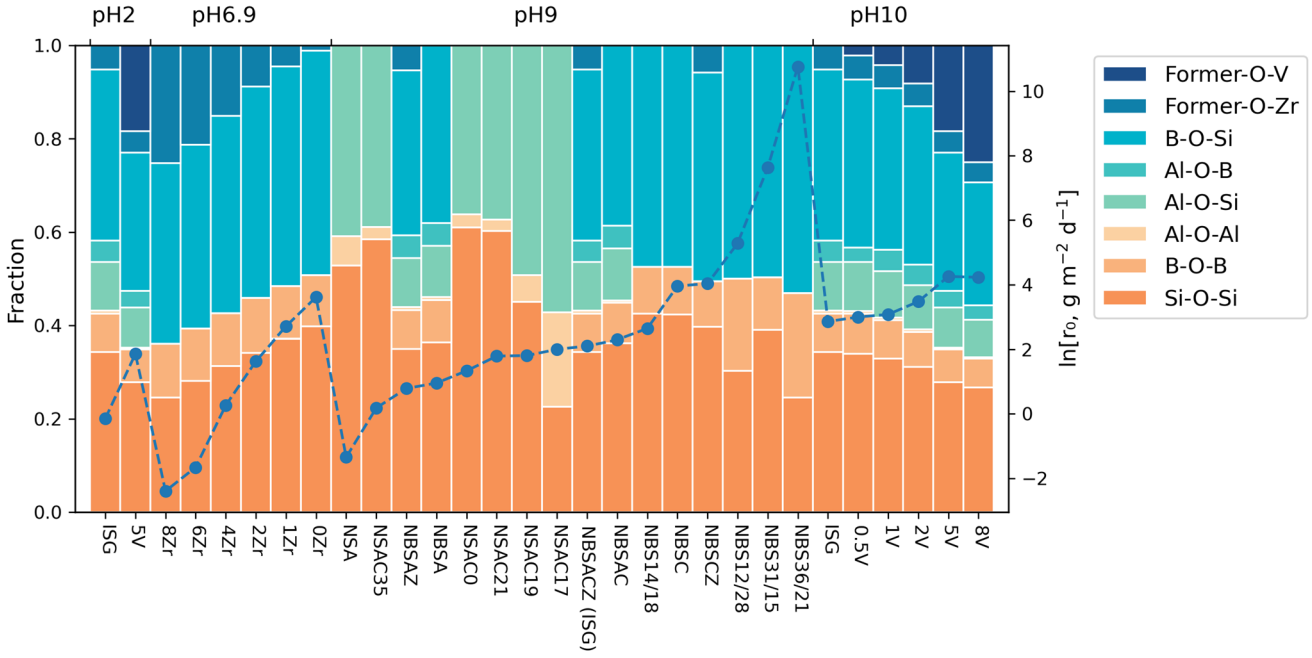

FIGURE 2 Stacked bar chart of polyhedral linkages and r_0 (blue dots) of the studied glasses

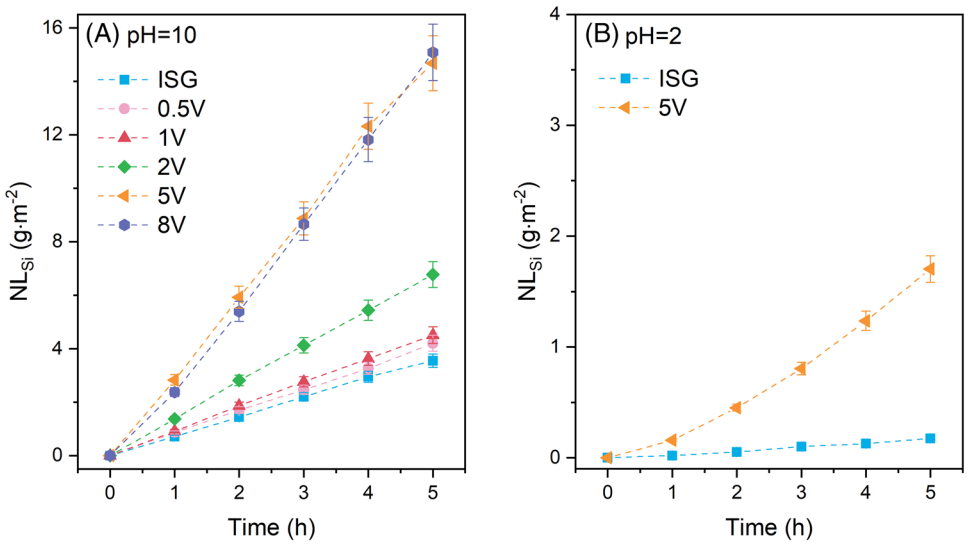

FIGURE 3 Normalized loss of Si (NL_{Si}) for the V series tested at $pH_{90°C} = 10$ (A) and 2 (B)

3.3 | Initial dissolution rate model

A linear model was fitted using the data with $pH_{90°C}$ between 6.9 and 10, where the dissolution rate values at $pH_{90°C} = 2$ were not used due to the issues discussed in the previous section. Table 2 lists the fitted model coefficients, standard errors of the coefficients (i.e., the standard deviation of the coefficients), and model-fit summary statistics. This model contains parameters, including pH, Al–O–B, Al–O–Si, Si–O–Si, former–O–Zr linkages, and percentages of non-bridging oxygen (NBO) among all the oxygen speciation (i.e., bridging oxygen, NBO, and tri-bridging oxygen) obtained from MD simulation. The coefficient of determination (R^2) and root mean square error (RMSE) of the model are 0.949 and 0.681, respectively. The model well represents the data fitted; however, the coefficients will likely need to be updated if applied to a wider compositional range and/or r_0 is measured under a larger pH range. R^2 press and R^2 adjusted are 0.887 and 0.935, respectively, which are slightly smaller than R^2 (0.949), indicating that no data points have a dominating effect in determining the fit of the model and that the model contains no unnecessary terms. R^2 adjusted and R^2 press can take negative values for a poor-fitting model that contains several

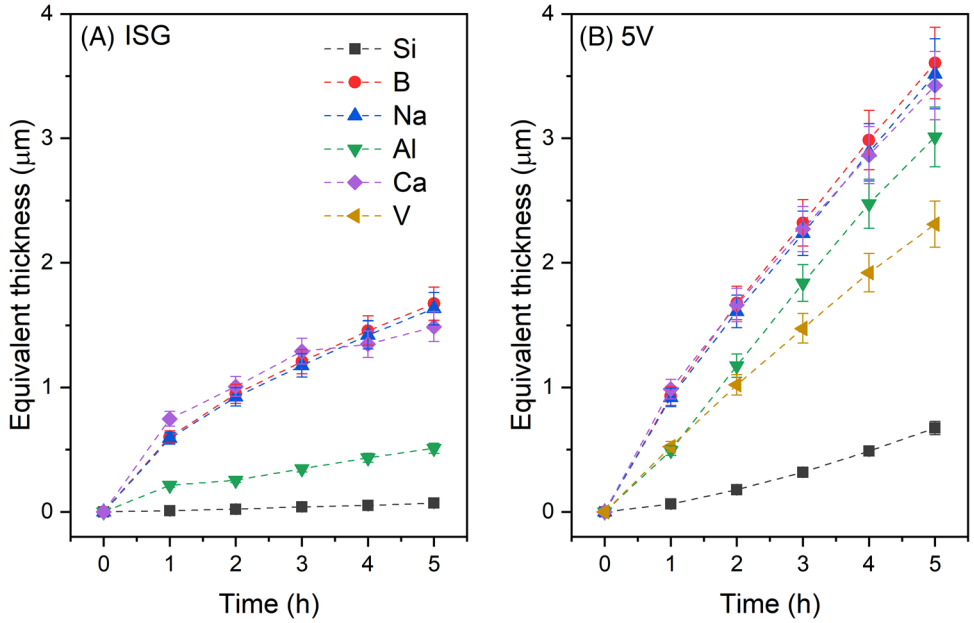

FIGURE 4 Equivalent thickness of International Simple Glass (ISG) (A) and 5 V (B) tested at $pH_{90°C} = 2$. Equivalent thickness at $pH_{90°C} = 10$ can be found in the SI section.

more terms than needed to fit the data or a model fitted to data with one or more very influential data points.[51] More detailed descriptions and equations of R^2, RMSE, R^2 adjusted, and R^2 press can be found in the SI section. In addition, nonlinear (higher order) and mixing effects were also evaluated, but they were ultimately found to be insignificant. Furthermore, linear and nonlinear models were fitted (also guided by stepwise regression) using glass compositions and pH as input parameters for this current dataset, where the highest R^2 was found to be 0.748 with an R^2 press of 0.438, and the highest R^2 press was found to be 0.548 with an R^2 of 0.682.

Figure 5 displays the predicted versus measured r_0 values, showing that this model can predict a wide range of r_0 without a bias. Figure 6 shows the predicted individual component effects on $\ln[r_0, \text{g m}^{-2} \text{d}^{-1}]$. Higher pH and NBO result in a higher r_0 value, whereas higher fractions of Al–O–B, Al–O–Si, Si–O–Si, and former–O–Zr linkages slightly decrease r_0. The Al–O–B term has a large model coefficient (−30.09) and a small component effect (i.e., a small negative slope shown in Figure 6), which is due to the small fraction (less than 5%) of Al–O–B in all the glasses. The Si-O-B and former-O-V linkages have a negligible impact on the model from stepwise regression analysis, based on the fact that they have high *p*-values indicating the insignificance of the model term and have no impact on R^2 and R^2 press values. However, these linkages can affect the dissolution rate calculations by changing the fractions of the other former-O-former linkages (e.g., reducing Si network connectivity hence smaller fraction for Si-O-Si linkage). The effects of vanadium oxide on glass properties have been experimentally confirmed previously, where 2 mol% V_2O_5 addition to ISG was found to reduce the glass transition temperature.[44]

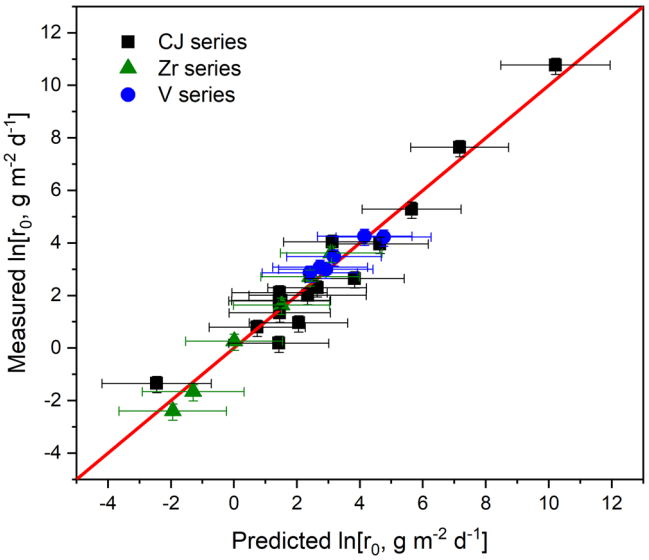

FIGURE 5 Predicted (error bars: 95% prediction interval) versus measured (error bars: 30% r_0[22]) plot of $\ln[r_0, \text{g m}^{-2} \text{d}^{-1}]$

4 | DISCUSSION

Various efforts have been conducted to develop models to predict r_0 using approaches such as machine learning, the application of the kinetic rate equation, TCT, and QSPR

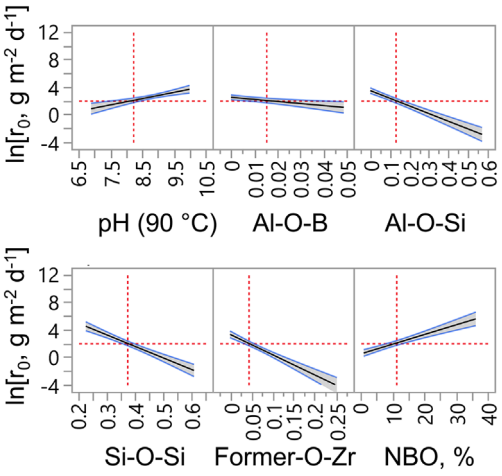

FIGURE 6 Predicted individual component effects on $\ln[r_0, \text{g m}^{-2}\text{ d}^{-1}]$

analysis with descriptors from MD simulation. Table 3 shows a comparison of a few example models and the one developed in this study. Anoop Krishnan et al.[29] and Lillington et al.[27] studied the ability of various machine learning algorithms to predict radioactive waste glass dissolution. Although some algorithms can achieve high accuracy, the model performance is highly dependent on input variables and data size. Additionally, machine learning approaches are prone to overfitting, and often without physical interpretation or insight of the results. The linear regression models based on the kinetic rate equation developed by Vienna et al.[10] provide chemically meaningful interpretations of the coefficients; however, the current models are only valid over composition region(s) applicable for waste vitrification.

Topological constraints from TCT are straightforward to calculate on the basis of glass composition. This approach is thus relatively easy to implement, leading to applications such as predicting glass properties,[52] including glass transition temperature,[53] thermal expansion coefficients,[54] Young's modulus,[55] and dissolution rates.[22,25] Even though this approach is simple, it does have a physical interpretation,[52] but with a significantly simplified picture of glass structure. In addition, it is challenging to obtain topological constraints (e.g., bond-bending and bond-stretching) for cations that have multiple oxidation states and coordination environments, interfering with its application on complex materials.[52]

The QSPR analysis based on MD results is another powerful method that can provide a clear physical interpretation of the results. The approach combines glass short-range structural information with energetics, such as bond strength in the structural descriptor such as F_{net}, and has been used to correlate glass properties, such as density,[35] thermal expansion coefficient,[35] mechanical properties,[35,56] and dissolution.[31–33] MD simulations with recent potential developments[49] provide detailed structural information such as cation coordination environments and glass former Q_n distributions; however, the application of this approach on complex materials is limited by unknown bond energy information (e.g., V^{4+}–O and V^{5+}–O bonds) and available MD potential parameters. Other descriptors based on the glass structure such as fraction of NBO, average network connectivity, and average ring size have also been explored as structural descriptors,[32] but none of the previous studies have used the statistics of network cation–oxygen-network cation linkages, a key information of the glass network structures.

In this study, we expand the QSPR analysis to use these network linkages. A linear regression model based on MD structure was developed and shown to provide accurate predictions of r_0 for a large range of glasses and pH values. The model coefficients can also be explained and have physical meanings. In order to identify the effect of pH further, more data in which several glasses are measured at a wider range of pH values are needed in the future modeling works. Even though the model's coefficients will likely need to be updated with data from a wider compositional space and pH range, the results of this work show that the approach is promising to provide simple calculations and accurate predictions of r_0. Density function theory calculations of various energy barriers[36,57] of breaking former linkages under basic, neutral, and acidic environments would improve the model in the future. However, a consistent set of energy barrier sets for the hydrolysis of various linkages is still lacking, as was summarized by Du and Rimsza.[36] Additionally, theoretical calculations of NBO for multicomponent glasses and polyhedral linkages based on MD simulation would greatly help to simplify the process of obtaining structural descriptors and accelerating the application of these models.

In terms of the effect of V_2O_5 on glass dissolution, Siligardi et al.[58] observed increasing dissolution rates with additions of 1 mol% V_2O_5 in Ca–Zr silicate glasses by testing with 2 g of glass powder in 50 ml stirred bi-distilled water at 98°C for 60 min. Their finding is consistent with the results in this study. Up to 4.09 wt% V_2O_5 additions to high-sodium (low activity waste) glasses have negligible to slightly positive effects (i.e., increasing) on product consistency test (PCT) and vapor hydration test (ASTM Method C1663[59]) responses.[51] However, the addition of V_2O_5 (2 mol%) was previously found to reduce the extent of ISG dissolution in a 112-day static dissolution test (surface-area-to-solution-volume ratio of 200 m^{-1} in a $\text{pH}_{25°\text{C}} = 7$ TRIS buffer solution).[60] This reduced dissolution may be due to the reaction of vanadate with either hydroxyl and amino functions of TRIS and the formation of V(V) complexes,[61] leading to a reduced pH at the end of the test comparing to the other samples without V_2O_5.

TABLE 3 Comparison of composition and structural models to predict r_0

Model	Examples	Model parameters	Advantages	Disadvantages
Composition-property model based on machine learning	Anoop Krishnan et al.[29] and Lillington et al.[27]	Glass chemical composition, temperature, and pH	• Can achieve high accuracy • Numerous machine learning algorithms are available	• Model accuracy is highly dependent on machine learning algorithm, model input variables, and data size • Prone to overfitting • Interpretation of chemical and physical phenomena is indirect
Linear regression based on kinetic rate equation parameters	Vienna et al.[10]	Intrinsic rate constant, pH coefficient, apparent activation energy, and component concentrations	• Simple interpretation of coefficients	• Currently only valid over composition region(s) applicable for waste vitrification
TCT	Gin et al.[22]	Bond-bending and bond-stretching constraints derived from coordination, BO, and NBO	• Theoretical calculation • Simple to implement	• Difficult (or less accurate) to obtain bond constraints for cations that have multiple oxidation states and coordination environments
MD-based QSPR	Du et al.[32]	Coordination and bond energy	• MD provides detailed coordination of cations • Other structural features (Q_n, NBO) can be included. • Includes bond energetic information	• Lack of bond energy information (e.g., V^{5+}–O and V^{4+}–O bond) • Limited by available MD potential parameters • Requires MD simulation for each glass composition
Linear regression based on MD structure	This study	pH, polyhedral linkages, and NBO	• Includes medium-range structural features • Can be used on a wide range of pH • Direct identification of structural influences	• Limited by available MD potential parameters • Requires MD simulation for each glass composition

Abbreviations: MD, molecular dynamics; NBO, non-bridging oxygen; TCT, topological constraint theory; QSPR, quantitative structure–property relationship.

Lian et al.[62] recently found that V_2O_5 can effectively suppress the crystallization tendency of $CaMoO_4$ and improve the solubility of MoO_3 in Mo-bearing aluminoborosilicate glass, while maintaining a low dissolution rates as compared to standard borosilicate waste glasses tested using the PCT.

Taken together, these results suggest that the impact of vanadium on glass corrosion is not the same across all the glass compositions and test conditions. This type of nonuniformity in impact was also observed for elements, such as Mg,[25,63] Al,[64,65] Zr,[66] and Zn.[67] For instance, Cailleteau et al.[66] discovered that substituting SiO_2 by ZrO_2 slows the initial dissolution rate, but ultimately leads to a greater degree of corrosion, due to the slower alteration layer formation and densification. The results of this study convincingly demonstrate that increasing V_2O_5 in glass changes the overall Si network connectivity and, hence, impacts r_0. Thus, glasses with different starting compositions/structures can lead to different impacts of V_2O_5 addition on r_0. V_2O_5 effects on residual rate (as indicated by longer term static tests) are likely due to either the impact on surface layer properties or activity of glass components in solution. Therefore, although the current model works well for initial dissolution rate prediction, in order to predict the residual rate, future models, including other structural and/or external parameters to predict alteration layer formation, are needed.

The r_0 data measured at $pH_{90°C} = 2$ were excluded from model fitting due to the nonlinear release of Si, leading to questions regarding how to define r_0 and how to correlate measured r_0 to glass structure in acid condition. If Si release is linear and maximum for a given temperature and pH, it is assumed that r_0 based on Si corresponds to the maximum rate for glass matrix dissolution (main glass network) regardless of the dissolution behavior of the other elements, such as B, Na, and Ca (i.e., congruent or incongruent). This is the case for the model developed in this study. However, when a glass dissolves incongruently and Si release is nonlinear, glass matrix dissolution corresponds to various factors (e.g., dissolution of the other elements, properties of the alteration layers, solution feedbacks); therefore, direct correlation of measured r_0 to glass bulk structure is no longer possible. Future work on the correlation of glass bulk structure—alteration layer formation—glass matrix dissolution under acid condition is thus needed.

5 | CONCLUSION

In this work, we propose a new model that is based on the statistics of network former–oxygen–network former linkages from MD simulations as a main descriptor for the initial dissolution rate prediction for a wide range of borosilicate glasses. The correlation between network former linkages and the initial dissolution rate r_0 measured at different pH values of a series of 28 glasses was studied. A high-fidelity linear model that provides good predictions without higher order or mixing terms was obtained using the linkages and NBO obtained from MD, with R^2 and RMSE values of 0.949 and 0.681, respectively. Higher pH and NBO result in a higher r_0, whereas higher fractions of Al–O–B, Al–O–Si, Si–O–Si, and former–O–Zr linkages slightly decrease r_0. Even though this model's coefficients likely need to be updated with data that have a wider compositional space and pH range, this approach is promising to provide simple calculations and accurate predictions of r_0. Future works should include consistent sets of hydrolysis energy barriers of these linkages, theoretical calculations of NBO, and polyhedral linkage types (e.g., corner versus edge sharing), which could further improve the model application.

ACKNOWLEDGMENTS

This work was supported as part of the Center for Performance and Design of Nuclear Waste Forms and Containers, an Energy Frontier Research Center funded by the U.S. Department of Energy (DOE), Office of Science, Basic Energy Sciences under Award # DESC0016584. Manuscript writing was also funded, in part, by a PNNL Laboratory Directed Research and Development effort. Pacific Northwest National Laboratory is a multi-program national laboratory operated for the U.S. Department of Energy by Battelle Memorial Institute under Contract DE-AC06-76RL01830.

The authors also thank James J Neeway (PNNL) and two anonymous reviewers for helpful comments that improved the manuscript.

ORCID

Xiaonan Lu https://orcid.org/0000-0001-7970-8148
Lu Deng https://orcid.org/0000-0002-5912-3908
Stéphane Gin https://orcid.org/0000-0002-1950-9195
Benjamin Parruzot https://orcid.org/0000-0002-2841-6660
Joelle T. Reiser https://orcid.org/0000-0002-2638-1580
Joseph V. Ryan https://orcid.org/0000-0002-2549-660X
John D. Vienna https://orcid.org/0000-0002-6832-9502
Jincheng Du https://orcid.org/0000-0003-4805-7498

REFERENCES

1. Hench LL. The story of bioglass. J Mater Sci Mater Med. 2006;17(11):967–78.
2. Frankel GS, Vienna JD, Lian J, Scully JR, Gin S, Ryan JV, et al. A comparative review of the aqueous corrosion of glasses, crystalline ceramics, and metals. NPJ Mater Degrad. 2018;2:15.

3. Gin S, Delaye J-M, Angeli F, Schuller S. Aqueous alteration of silicate glass: state of knowledge and perspectives. NPJ Mater Degrad. 2021;5(1):1–20.
4. Gin S, Abdelouas A, Criscenti LJ, Ebert WL, Ferrand K, Geisler T, et al. An international initiative on long-term behavior of high-level nuclear waste glass. Mater Today. 2013;16(6):243–8.
5. Vienna JD, Ryan JV, Gin S, Inagaki Y. Current understanding and remaining challenges in modeling long-term degradation of borosilicate nuclear waste glasses. Int J Appl Glass Sci. 2013;4(4):283–94.
6. Frankel GS, Vienna JD, Lian J, Guo X, Gin S, Kim SH, et al. Recent advances in corrosion science applicable to disposal of high-level nuclear waste. Chem Rev. 2021;121(20):12327–83.
7. Inagaki Y, Kikunaga T, Idemitsu K, Arima T. Initial dissolution rate of the International Simple Glass as a function of pH and temperature measured using microchannel flow-through test method. Int J Appl Glass Sci. 2013;4(4):317–27.
8. Fournier M, Gin S, Frugier P. Resumption of nuclear glass alteration: state of the art. J Nucl Mater. 2014;448(1–3):348–63.
9. Gin S, Jollivet P, Fournier M, Berthon C, Wang Z, Mitroshkov A, et al. The fate of silicon during glass corrosion under alkaline conditions: a mechanistic and kinetic study with the International Simple Glass. Geochim Cosmochim Acta. 2015;151:68–85.
10. Vienna JD, Neeway JJ, Ryan JV, Kerisit SN. Impacts of glass composition, pH, and temperature on glass forward dissolution rate. NPJ Mater Degrad. 2018;2(1):22.
11. Neeway J, Abdelouas A, Grambow B, Schumacher S, Martin C, Kogawa M, et al. Vapor hydration of SON68 glass from 90°C to 200°C: a kinetic study and corrosion products investigation. J Non-Cryst Solids. 2012;358(21):2894–905.
12. Ferrand K, Abdelouas A, Grambow B, Crovisier J-L. The role of water diffusion in the corrosion of the French nuclear waste glass SON 68 under solution saturation conditions. MRS Proc. 2003;807:193.
13. De Echave T, Tribet M, Gin S, Jégou C. Influence of iron on the alteration of the SON68 nuclear glass in the Callovo-Oxfordian groundwater. Appl Geochem. 2019;100:268–78.
14. Lenting C, Plümper O, Kilburn M, Guagliardo P, Klinkenberg M, Geisler T. Towards a unifying mechanistic model for silicate glass corrosion. NPJ Mater Degrad. 2018;2(1):28.
15. Backhouse DJ, Fisher AJ, Neeway JJ, Corkhill CL, Hyatt NC, Hand RJ. Corrosion of the International Simple Glass under acidic to hyperalkaline conditions. NPJ Mater Degrad. 2018;2(1):29.
16. Aréna H, Godon N, Rébiscoul D, Podor R, Garcès E, Cabie M, et al. Impact of Zn, Mg, Ni and Co elements on glass alteration: additive effects. J Nucl Mater. 2016;470:55–67.
17. Collins DR, Catlow CRA. Computer simulation of structures and cohesive properties of micas. Am Mineral. 1992;77(11–12):1172–81.
18. Thorpe CL, Neeway JJ, Pearce CI, Hand RJ, Fisher AJ, Walling SA, et al. Forty years of durability assessment of nuclear waste glass by standard methods. NPJ Mater Degrad. 2021;5, https://doi.org/10.1038/s41529-021-00210-4
19. Fournier M, Ull A, Nicoleau E, Inagaki Y, Odorico M, Frugier P, et al. Glass dissolution rate measurement and calculation revisited. J Nucl Mater. 2016;476:140–54.
20. ASTM C1662-18. Standard practice for measurement of the glass dissolution rate using the single-pass flow-through test method. West Conshohocken, PA: ASTM International; 2018.
21. Kaspar TC, Ryan JV, Pantano CG, Rice J, Trivelpiece C, Hyatt NC, et al. Physical and optical properties of the International Simple Glass. NPJ Mater Degrad. 2019;3:15.
22. Gin S, Wang M, Bisbrouck N, Taron M, Lu X, Deng L, et al. Can a simple topological-constraints-based model predict the initial dissolution rate of borosilicate and aluminosilicate glasses? NPJ Mater Degrad. 2020;4(1):6.
23. Neeway JJ, Rieke PC, Parruzot BP, Ryan JV, Asmussen RM. The dissolution behavior of borosilicate glasses in far-from equilibrium conditions. Geochim Cosmochim Acta. 2018;226:132–48.
24. Pignatelli I, Kumar A, Bauchy M, Sant G. Topological control on silicates' dissolution kinetics. Langmuir. 2016;32(18):4434–9.
25. Bisbrouck N, Micoulaut M, Delaye JM, Gin S, Angeli F. Structure-property relationship and chemical durability of magnesium-containing borosilicate glasses with insight from topological constraints. NPJ Mater Degrad. 2022;6(1):58.
26. Han T, Stone-Weiss N, Huang J, Goel A, Kumar A. Machine learning as a tool to design glasses with controlled dissolution for healthcare applications. Acta Biomater. 2020;107:286–98.
27. Lillington JNP, Goût TL, Harrison MT, Farnan I. Predicting radioactive waste glass dissolution with machine learning. J Non-Cryst Solids. 2020;533:119852.
28. Liu H, Zhang T, Anoop Krishnan NM, Smedskjaer MM, Ryan JV, Gin S, et al. Predicting the dissolution kinetics of silicate glasses by topology-informed machine learning. NPJ Mater Degrad. 2019;3:32.
29. Anoop Krishnan NM, Mangalathu S, Smedskjaer MM, Tandia A, Burton H, Bauchy M. Predicting the dissolution kinetics of silicate glasses using machine learning. J Non-Cryst Solids. 2018;487:37–45.
30. Linati L, Lusvardi G, Malavasi G, Menabue L, Cristina Menziani M, Mustarelli P, et al. Qualitative and quantitative structure—property relationship analysis of multicomponent potential bioglasses. J Phys Chem B. 2005;109(11):4989–98.
31. Lusvardi G, Malavasi G, Tarsitano F, Menabue L, Menziani MC, Pedone A. Quantitative structure-property relationships of potentially bioactive fluoro phospho-silicate glasses. J Phys Chem B. 2009;113(30):10331–8.
32. Du J, Lu X, Gin S, Delaye J-M, Deng L, Taron M, et al. Predicting the dissolution rate of borosilicate glasses using QSPR analysis based on molecular dynamics simulations. J Am Ceram Soc. 2021;104(9):4445–58.
33. Lu X, Deng L, Gin S, Du J. Quantitative structure–property relationship (QSPR) analysis of ZrO_2-containing soda-lime borosilicate glasses. J Phys Chem B. 2019;123:1412–22.
34. Pedone A, Menziani MC. Computational modeling of silicate glasses: a quantitative structure-property relationship perspective. Springer Ser Mater Sci. 2015;215:113–35.
35. Lu X, Du J. Quantitative structure-property relationship (QSPR) analysis of calcium aluminosilicate glasses based on molecular dynamics simulations. J Non-Cryst Solids. 2020;530:119772.
36. Du J, Rimsza JM. Atomistic computer simulations of water interactions and dissolution of inorganic glasses. NPJ Mater Degrad. 2017;1:16.
37. Nagamine K, Honma T, Komatsu T. Selective synthesis of lithium ion-conductive β-$LiVOPO_4$ crystals via glass-ceramic processing. J Am Ceram Soc. 2008;91(12):3920–5.
38. Afyon S, Krumeich F, Mensing C, Borgschulte A, Nesper R. New high capacity cathode materials for rechargeable Li-ion batteries: vanadate-borate glasses. Sci Rep. 2014;4(1):1–7.

39. McKeown DA, Muller IS, Matlack KS, Pegg IL. X-ray absorption studies of vanadium valence and local environment in borosilicate waste glasses using vanadium sulfide, silicate, and oxide standards. J Non-Cryst Solids. 2002;298(2–3):160–75.
40. Sengupta P, Dey KK, Halder R, Ajithkumar TG, Abraham G, Mishra RK, et al. Vanadium in borosilicate glass. J Am Ceram Soc. 2015;98(1):88–96.
41. McKeown DA, Muller IS, Gan H, Feng Z, Viragh C, Pegg IL. Vanadium and chromium redox behavior in borosilicate nuclear waste glasses. J Non-Cryst Solids. 2011;357(14):2735–43.
42. Manara D, Grandjean A, Pinet O, Dussossoy JL, Neuville DR. Sulfur behavior in silicate glasses and melts: implications for sulfate incorporation in nuclear waste glasses as a function of alkali cation and V_2O_5 content. J Non-Cryst Solids. 2007;353(1):12–23.
43. Vienna JD, Kim D-S, Muller IS, Piepel GF, Kruger AA. Toward understanding the effect of low-activity waste glass composition on sulfur solubility. J Am Ceram Soc. 2014;97(10):3135–42.
44. Lu X, Sun R, Huang L, Ryan JV, Vienna JD, Du J. Effect of vanadium oxide addition on thermomechanical behaviors of borosilicate glasses: toward development of high crack resistant glasses for nuclear waste disposal. J Non-Cryst Solids. 2019;515:88–97.
45. Lu X, Deng L, Saslow SA, Liu H, Benmore CJ, Parruzot BP, et al. Vanadium oxidation states and structural role in aluminoborosilicate glasses: an integrated experimental and molecular dynamics simulation study. J Phys Chem B. 2021;125(44):12365–77.
46. Bergeron B, Galoisy L, Jollivet P, Angeli F, Charpentier T, Calas G, et al. First investigations of the influence of IVB elements (Ti, Zr, and Hf) on the chemical durability of soda-lime borosilicate glasses. J Non-Cryst Solids. 2010;356:2315–22.
47. Du J, Cormack A. Atomistic simulations of glasses. Hoboken, NJ: Wiley; 2022.
48. Deng L, Du J. Development of boron oxide potentials for computer simulations of multicomponent oxide glasses. J Am Ceram Soc. 2019;102:2482–505.
49. Deng L, Lu X, Vienna JD, Du J. Structures of vanadium-containing silicate and borosilicate glasses: vanadium potential development and MD simulations. J Non-Cryst Solids. 2022;575:121223.
50. Kaya H, Ngo D, Smith NJ, Gin S, Kim SH. Network structure in alteration layer of boroaluminosilicate glass formed by aqueous corrosion. J Non-Cryst Solids. 2020;553:120494.
51. Vienna JD, Heredia-Langner A, Cooley SK, Holmes AE, Kim D-S, Lumetta NA. Glass property-composition models for support of Hanford WTP LAW facility operation. Richland, Washington: Pacific Northwest National Laboratory; 2022. PNNL-30932, Rev. 2
52. Bauchy M. Deciphering the atomic genome of glasses by topological constraint theory and molecular dynamics: a review. Comput Mater Sci. 2019;159:95–102.
53. Bødker MS, Mauro JC, Youngman RE, Smedskjaer MM. Statistical mechanical modeling of borate glass structure and topology: prediction of superstructural units and glass transition temperature. J Phys Chem B. 2019;123:1206–13.
54. Zeng H, Ye F, Li X, Wang L, Yang B, Chen J, et al. Calculation of thermal expansion coefficient of glasses based on topological constraint theory. Chem Phys Lett. 2016;662:268–72.
55. Yang K, Yang B, Xu X, Hoover C, Smedskjaer MM, Bauchy M. Prediction of the Young's modulus of silicate glasses by topological constraint theory. J Non-Cryst Solids. 2019;514:15–9.
56. Kuo P, Du J. Atomistic understanding of ion exchange strengthening of boroaluminosilicate glasses: insights from molecular dynamics simulations and QSPR analysis. J Phys Chem B. 2022;126(9):2060–72.
57. Zapol P, He H, Kwon KD, Criscenti LJ. First-principles study of hydrolysis reaction barriers in a sodium borosilicate glass. Int J Appl Glass Sci. 2013;4(4):395–407.
58. Siligardi C, Ferrari AM, Leonelli C, Bruni S. Vanadium doping in $CaO–ZrO_2–SiO_2$ glasses. Phys Chem Glasses. 2002;43(2):97–101.
59. ASTM C1663-18. Standard test method for measuring waste glass or glass ceramic durability by vapor hydration test. West Conshohocken, PA: ASTM International; 2018.
60. Lu X, Neeway JJ, Ryan JV, Du J. Influence of low concentration V and Co oxide doping on the dissolution behaviors of simplified nuclear waste glasses. J Non-Cryst Solids. 2016;452:161–8.
61. Tracey AS, Gresser MJ. Vanadium(V) oxyanions: interactions of vanadate with 1,1,1-tris(hydroxymethyl)ethane and with the buffer tris(hydroxymethyl)aminomethane. Inorg Chem. 1988;27(7):1269–75.
62. Lian Q, Zhang X, Ji H, Yu P, Guo X, Wan W, et al. Effect of V_2O_5 on crystallization tendency and chemical durability of Mo-bearing aluminoborosilicate glass. Mater Res Express. 2020;7(4):045201.
63. Debure M, Frugier P, De Windt L, Gin S. Borosilicate glass alteration driven by magnesium carbonates. J Nucl Mater. 2012;420(1–3):347–61.
64. Vienna JD, Crum JV. Non-linear effects of alumina concentration on product consistency test response of waste glasses. J Nucl Mater. 2018;511:396–405.
65. Damodaran K, Delaye JM, Kalinichev AG, Gin S. Deciphering the non-linear impact of Al on chemical durability of silicate glass. Acta Mater. 2022;225:117478.
66. Cailleteau C, Algeli F, Devreux F, Gin S, Jestin J, Jollivet P, et al. Insight into silicate-glass corrosion mechanisms. Nat Mater. 2008;7(12):978–83.
67. Gin S, Frugier P, Jollivet P, Bruguier F, Curti E. New insight into the residual rate of borosilicate glasses: effect of S/V and glass composition. Int J Appl Glass Sci. 2013;4(4):371–82.

SUPPORTING INFORMATION

Additional supporting information can be found online in the Supporting Information section at the end of this article.

How to cite this article: Lu X, Deng L, Gin S, Parruzot B, Reiser JT, Ryan JV, et al. Predicting initial dissolution rates using structural features from molecular dynamics simulations. J Am Ceram Soc. 2022;1–12. https://doi.org/10.1111/jace.18850